Noise reduction potential of flow permeable materials for jet-flap interaction noise

Christian Jente*, Johannes Schmidt†, Jan W. Delfs‡,

Karl-Stéphane Rossignol§, Michael Pott-Pollenske¶, Henri Siller‖

German Aerospace Center (DLR), Lilienthalplatz 7, D-38108 Braunschweig, Germany

Jet-flap interaction (JFI) noise plays a particularly important role during take-offs and landings, i.e. when the aircraft is in the immediate vicinity of inhabited areas.

The interaction of the jet with the deployed flaps causes a substantial increase of low-frequent aircraft noise. Noise reduction technologies (NRTs) were studied for their potential to diminish the JFI effect: The wing was equipped with various permeable or porous (flap) trailing edges which cover the last 10% of the clean chord length.

The first test was conducted at the Aeroacoustic Wind tunnel in Braunschweig (AWB) on a cruise wing model, i.e. the engine was not installed. Beneath the testing of various materials and concepts, a design parameter study was conducted about the minimally needed treated chord length.

The four most promising materials were down-selected for an installed engine test at the jet noise test facility JExTRA in Berlin: Two NRTs are designed as hollow flaps: perforated or slotted metal sheets are fixed onto a rib structure. The other two NRTs are porous materials (fine/coarse size). The tests were conducted for static operations between Mj=0.45 and 0.75. The engine integration was mainly defined by a height of H=0.6Dj (close integration) and a length of L=2Dj.

Remarkable noise reduction was measured especially for low jet Mach numbers and up to Mj=0.7. At high Mach number, some NRTs produce tones which follow a Helmholtz analogy. The only tested NRT which is immune to this, uses a cover mesh which introduces another trailing edge.

The tests with flow permable flap trailing edges show the great potential of reducing jet-flap interaction noise. Open questions regard (1) the deepening of the physical understanding of noise reduction mechanisms, (2) a proof of performance under flight conditions and (3) a design optimization which balances a small aerodynamic lift penalty vs. the acoustic benefit.

*Research Engineer, Department of Technical Acoustics, Institute of Aerodynamics and Flow Technology, christian.jente@dlr.de

†Research Engineer, Technical Acoustics, Institute of Aerodynamics and Flow Technology, johannes.schmidt@dlr.de

‡Head of Department, Technical Acoustics, Institute of Aerodynamics and Flow Technology, jan.delfs@dlr.de

§Research Engineer, Technical Acoustics, Institute of Aerodynamics and Flow Technology, karl-stephane.rossignol@dlr.de

¶Research Engineer, Technical Acoustics, Institute of Aerodynamics and Flow Technology, michael.pott-pollenske@dlr.de

‖Research Engineer, Engine Acoustics, Institute of Propulsion Technology, DLR Berlin, Müller-Breslau-Str. 8, D-10623 Berlin, Germany, henri.siller@dlr.de

Nomenclature

δ_ω	[°]	thickness of near-field shear layer
α_{geo}	[°]	incidence (geometric installation angle)
Δf	[Hz]	narrowband frequency bandwidth
ϕ'	[°]	half jet opening angle
ψ	[°]	azimuthal angle, from flyover arc
θ	[°]	polar angle, front-aft
a_∞	[m/s]	speed of sound
c	[m]	chord length
d	[m]	wire diameter
D_j	[m]	jet diameter
f	[Hz]	frequency
H	[m]	engine integration height
He	[-]	Helmholtz number
L	[m]	engine integration length
$L*$	[m]	characteristical length
L_0	[m]	virtual engine integration length
M_j	[-]	(jet) Mach number
$OASPL$	[dB]	overall sound pressure level
r_U	[-]	velocity ratio between U_∞ and U_j
R	[m]	microphone distance
R_j	[m]	jet radius
SPL	[dB]	sound pressure level
SPL_{nb}	[dB]	narrowband sound pressure level
Sr	[-]	Strouhal number
T_0	[K]	Test room temperature
U	[m/s]	streamwise velocity
U_∞	[m/s]	flight velocity
U_j	[m/s]	jet velocity
W	[m]	mesh width
x	[m]	streamwise coordinate
x_0	[m]	virtual shear layer origin
y, z	[m]	spanwise coordinate

AWB	Aeroacoustic Windtunnel Braunschweig
BL	solid "baseline" flap (w/o noise reduction technology)
DJ	*DJINN*, an EU research project
DLR	Deutsches Zentrum für Luft- und Raumfahrt e.V., i.e. the German Aerospace Center
ENG	centerpoint of engine (bypass) nozzle outlet, a measurement reference point
F16	name of a generic wing model
JFI	jet-flap interaction
MPP	microperforated plate
NF	*here:* the aerodynamic near-field of the jet
NRT	noise reduction technology
PA	porous aluminium
S/L	shear layer
w/o	without

I. AWB test of NRT potential on cruise wing model

The first test campaign was conducted at the Acoustic Wind Tunnel Braunschweig (AWB) in 2019 and is documented by Schmidt.[1] AWB is a low-speed open-jet test facility which produces velocities up to $U_\infty = 60\,\mathrm{m/s}$ downstream its rectangular wind tunnel nozzle outlet of size 0.8 m (width) × 1.2 m (height). The semi-anechoic test chamber is optimized for broadband noise frequencies above 250 Hz.[2]

An F16 cruise wing model was installed which contains a removable trailing edge. This enables the implementation of inserts which contain different noise reduction technologies (NRTs). The effective dimensions of the NRT insert is $b_{NRT} = 300\,\mathrm{mm}$ in spanwise direction and $c_{NRT} = 30\,\mathrm{mm}$ in chordwise direction. The permeable part thus corresponds to 10% of the chord length.[3]

The here discussed NRTs follow one of two concepts, the hollow flap or porous flap concept. **The hollow flap** is created by glueing or welding a thin metal sheet onto a rib structure and thereby enclosing an air cavity. The equal distribution of 7 ribs along the NRT span creates 6 larger compartments. In acoustic liner terminology, the porous metal sheet is called a face sheet. Yet, the here tested concept has no backing skin (other than the opposing face sheet). Hence, the analogy to a liner is not perfect. The face sheet has been realized by using two types of microperforated plates (MPP):

- NRT1 ■ (in former publications[3] also known as MPP3) contains round microperforations of diameter $100\,\mu\mathrm{m}$.
- NRT2 ■ (in former publications[3] also known as MPP1) contains slotted microperforations. One slotted or oblonged holes is defined by its short side of diameter $100\,\mu\mathrm{m}$ and long size length of $1100\,\mu\mathrm{m}$. Several oblonged holes are arranged in 15 rows along the NRT chord length. The long side is aligned with the streamwise flow direction. Note, that a spanwise alignment enhances the NRT performance,[3] especially for high frequencies.

The trailing edge of the microperforated plates are not defined by a solid line. The perforation is cut along the porous part which produces a regular serrated or cogged geometry. However, the sheet thickness is much larger than the cogged geometry. Hence, there is a fundamental difference to conventionally designed serrations where the zig-zag pattern is large in comparison to its thickness.

The **porous flap concept** is defined by rather randomly distributed cavities within the entire volume of the NRT-treated section of the trailing edge insert. The pore size results out of the manufacturing process where aluminium is casted onto crystal salt of a certain grain size. The salt is washed out and cavities remain which are larger in dimension than the grain size.

- NRT4 ■ (also known as PA80-110) was made out of a salt grain size which passes the filter grade of $80 \ldots 110\,\mu\mathrm{m}$. Since this is smaller than the salt grain size of NRT3, it is here referred to as the *fine* porous NRT. The washed out cavities have a pore size of up to $1000\,\mu\mathrm{m}$. The trailing edge is characterized by a rather irregular spanwise shape and a rather thin trailing edge (compared to other NRTs).
- NRT3 ■ was made out of a salt grain size which passes a filter grade of $200 \ldots 250\,\mu\mathrm{m}$, and is therefore here referred to as the *coarse* porous NRT. It is a graded material which means that there is a porosity gradient in chordwise direction (PA200-250 graded).

  With the addition of the cover mesh B (wire diameter $d \approx 50\,\mu\mathrm{m}$, mesh width $\approx 120\,\mu\mathrm{m}$), NRT3 becomes a hybrid concept: The mesh can be interpreted as a very porous face sheet. Furthermore, it is technically challenging to produce a cover mesh which is true to the geometry of the porous insert, since the mesh needs to be folded twice and must cover exactly the finite length of the porous trailing edge. The simpler solution is just one clean folding (compare figure 5). This creates a second "mesh" trailing edge and encompasses an air cavity between the porous trailing edge and the mesh trailing edge. This means that in chordwise direction there is an initial transition between solid and porous volume and another transition between porous volume and air cavity.
  The folding of the mesh induces micro-serrations at the trailing edge. Depending on the folding, the streamwise dimension can be half a mesh width, while the spanwise length is a full mesh width plus the wire thickness. The trailing edge thickness is similar to the wire thickness.

An elliptic mirror (figure 2) with a reflective diameter of 1.4 m was installed at the pressure side of the cruise wing. Its 1/4" Brüel&Kjær microphone is located at a distance of $R = 1150\,\mathrm{mm}$ to the trailing edge.

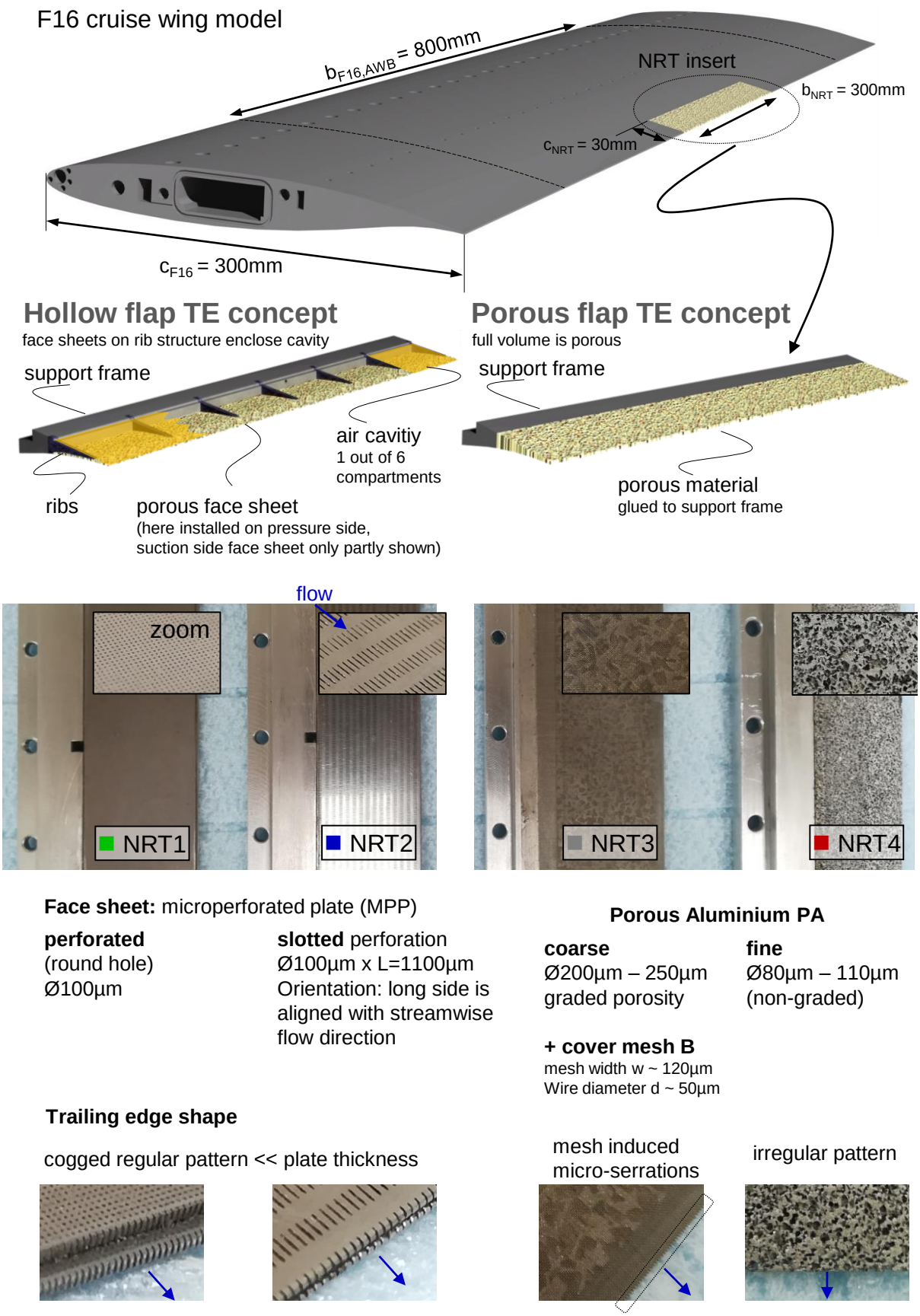

Figure 1: Noise reduction technologies implemented at F16 cruise wing trailing edge for AWB experiment.

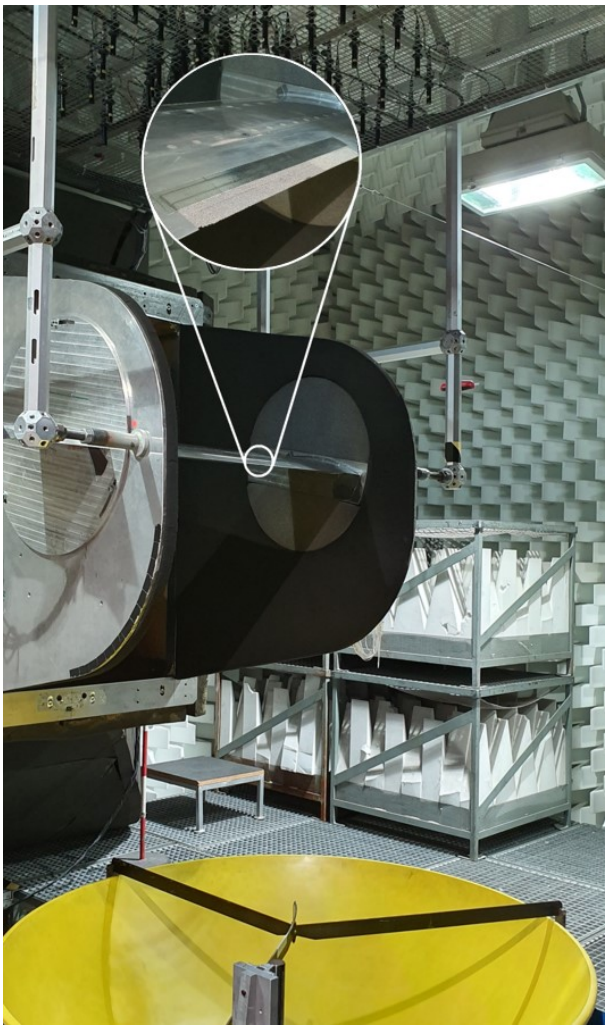

Figure 2: AWB setup 2019: elliptic mirror located below an F16 cruise wing.

A. General acoustic behaviour of NRTs on cruise wing

Flow permeable trailing edges reduce low-frequent noise, yet can increase high-frequent noise (see figure 3). The more permeable the trailing edges are, the greater is the low-frequent noise reduction. Unfortunately, the design of permeable structures comes often with a rougher surface: Take for example the coarse porous trailing edge PA250 which generates additional high-frequent noise (gray dashed line) - compared to both, the solid baseline (thick black) as well as a fine porous trailing edge (red). Yet, a fine cover mesh on top of the otherwise coarse porous material (gray solid line) reduces the surface resistance and thus the high-frequent noise. Smoother surface properties can be realized with hollow flap designs where perforated (green) or slotted (blue) metal sheets are fixed onto a rib structure. Especially the perforated trailing edge looks promising: The NRT produces a significant low-frequent noise benefit while causing no additional noise penalty to the reference trailing edge.

B. Design study: Influence of porous chord length

The influence of the chordwise porous length was investigated on a PA120 trailing edge. The porous material was covered with high-speed tape on both the pressure side and suction side (see figure 4).

In order to exclude the possibility that there is flow under the tape which influences the sound pressure level, one porous NRT was impregnated with glue/resin over the length of 75%. This allowed to compare the reduction of porous chord length by a proper solidifying volumetric treatment (glue) vs. the surface treatment (tape). The measured spectra of the volume and surface treated trailing edges are very similar (see Schmidt[1]). This result is hope for the conduction of non-destructive porous chord length studies.

The reduction of chordwise porous length due to addition of Alu tape causes a high-frequent noise reduction. This is in agreement with the aforementioned hypothesis that lower surface roughness produces

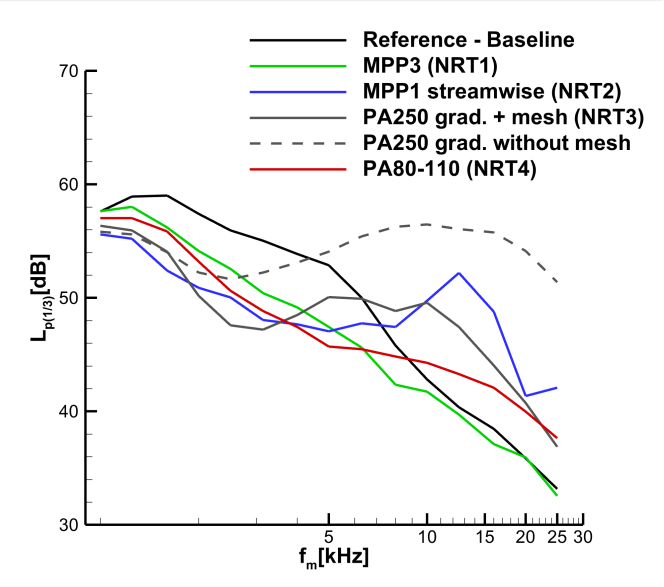

Figure 3: SPL of different trailing edges[1] ; $U_\infty = 50\,\mathrm{m/s}$; $\alpha_g = 0°$

chordwise tape length / NRT length			-0%	-25%	-50%	-75%
permeable chord length		c_{NRT}	30 mm	22.5 mm	15 mm	7.5 mm
relative permeable chord length wrt	F16 cruise wing $c_{F16} = 300\,\mathrm{mm}$	c_{NRT}/c_{F16}	10%	8%	5%	3%
	F16 flap $c_{flap} = 82\,\mathrm{mm}$	c_{NRT}/c_{flap}	36%	27%	18%	9%
	DJINN wing $c_{DJ} = 150\,\mathrm{mm}$	c_{NRT}/c_{DJ}	20%	–	–	–

Table 1: Variation of permeable NRT chord length

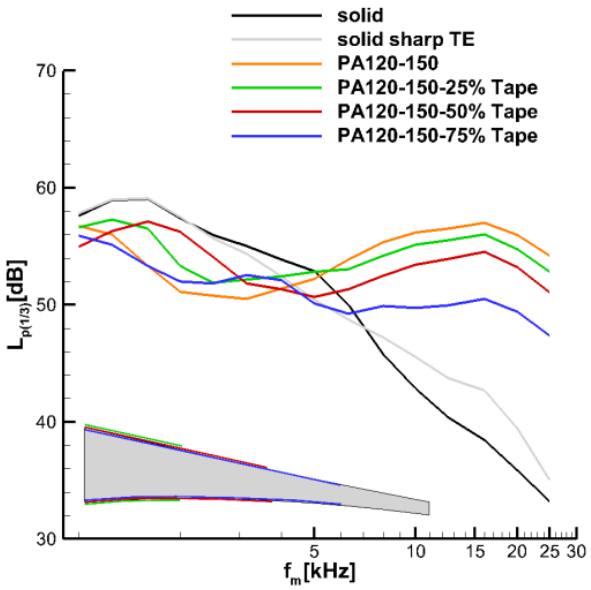

Figure 4: Chordwise NRT length effect, tested by high-speed taping[1] ; $U_\infty = 50\,\mathrm{m/s}$; $\alpha_g = 0°$

less noise (figure 4). Fortunately, the low frequent noise benefit is mostly preserved. This rather unexpected result shows that noise benefits can be achieved even with rather low porous length. Hence there is some design space to optimize porous lengths on a cruise wing model in order to keep lift penalties to a minimum.

Future studies may need to focus on the research question whether the positive effect due to shortening the treated chord length does apply (a) for the high-lift wing with and w/o an installed engine and (b) for materials that produce low high-frequent noise penalty anyway: It must be noted that the PA120 material produces a rather high high-frequent noise penalty compared to the solid trailing edge (figure 3). The performance of other materials and NRT concepts remains to be tested.

II. Installed jet test at JExTRA on statically operated high-lift setup

The installed jet experiments were conducted at DLR Berlin's jet noise facility JExTRA[4] in the summer of 2021. Contrary to the cruise wing integration of 2019, the selected porous trailing edges were attached to a F16 flap of span $b = 300\,\text{mm}$ and installed at a flap deflection angle of $\delta_F = 25\,°$. The flap was positioned with a form-fit flap holder (figure 6) which allowed to fine-adjust the flap deflection angle δ_F, engine integration length L and height H. Since the main wing merely serves as a reflective surface when there is no flight speed, the main wing element was substituted by a wooden plate. Jet flow of jet diameter $D_j = 50\,\text{mm}$ and jet Mach number $M_j = 0.45 \ldots 0.75$ was issued from a single stream jet nozzle into the slightly too warm test room $T_0 = \text{ISA} + 10 \ldots 20\,\text{K}$.

Beneath a baseline flap, the four different trailing edges (see figure 1) were investigated. The adjustment of NRT3 was conducted wrt. the academically correct mesh trailing edge (figure 5). The mechanical correct version (alignment to porous trailing edge) would have been more appropriate for the test.

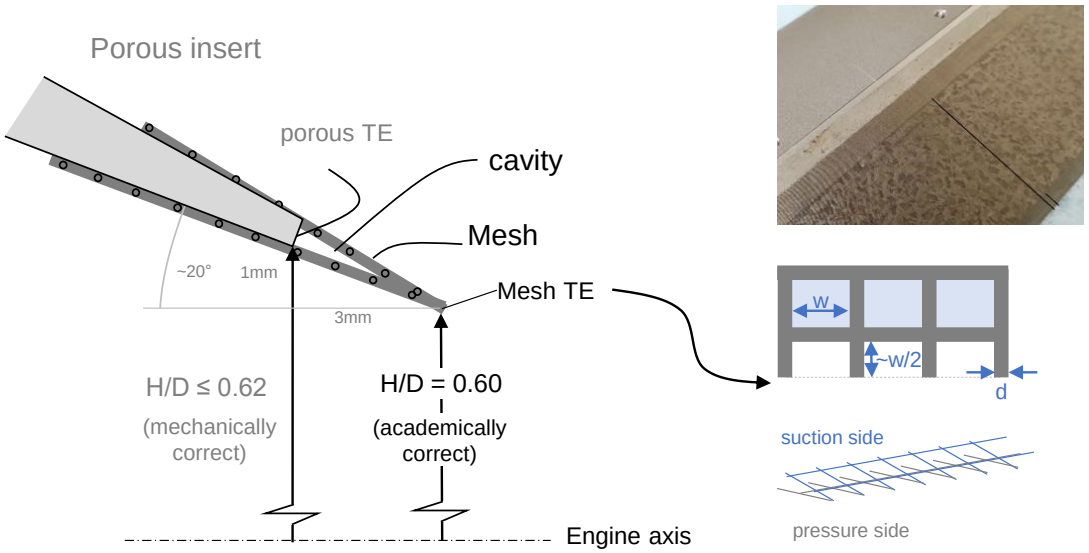

Figure 5: Engine integration options of NRT3 at porous TE or mesh TE.

The modified flap consists of a leading edge, a support structure and a porous trailing edge, which can be replaced.
Free-field microphones of type Microtech MK301 were installed in DLR Berlin's acoustic test environment "Stargate".

A. Evaluation with tone removal tool

The jet flap interaction (JFI) noise ΔSPL_{JFI} is determined for static operations as the difference between the installed and isolated engine (see also figure 9). The highest JFI noise is measured by the installed Baseline (BL) configuration (equation 1). This JFI noise (equation 2) can be reduced if an NRT is installed. Yet the reduced JFI noise is arguably less interesting than the noise reduction (equation 3). This is the reason why the following plots will show the noise reduction potential (BL JFI noise, equation 1) and compare it against the actual achieved noise reduction (equation 3). In the theoretical case that the JFI noise is fully eliminated, both curves match.

$$\text{BL JFI effect: } \Delta SPL_{BL.JFI} = OASPL_{BL.installed} - OASPL_{isolated.jet} \tag{1}$$

$$\text{NRT JFI effect: } \Delta OASPL_{NRT.JFI} = OASPL_{NRT.installed} - OASPL_{isolated.jet} \tag{2}$$

$$\text{Noise reduction: } \Delta OASPL_{reduct.} = OASPL_{BL.installed} - OASPL_{NRT.installed} \begin{cases} > 0 & \text{reduction} \\ < 0 & \text{penalty} \end{cases} \tag{3}$$

Before any noise reduction evaluations can be made, the JFI noise itself needs to be assessed and clustered into suitable physical sub-divisions. JFI noise can be divided into three frequency ranges, i.e. low, mid and high.[5] This is displayed very well in figure 7 where JFI noise is portrayed for various jet speeds at

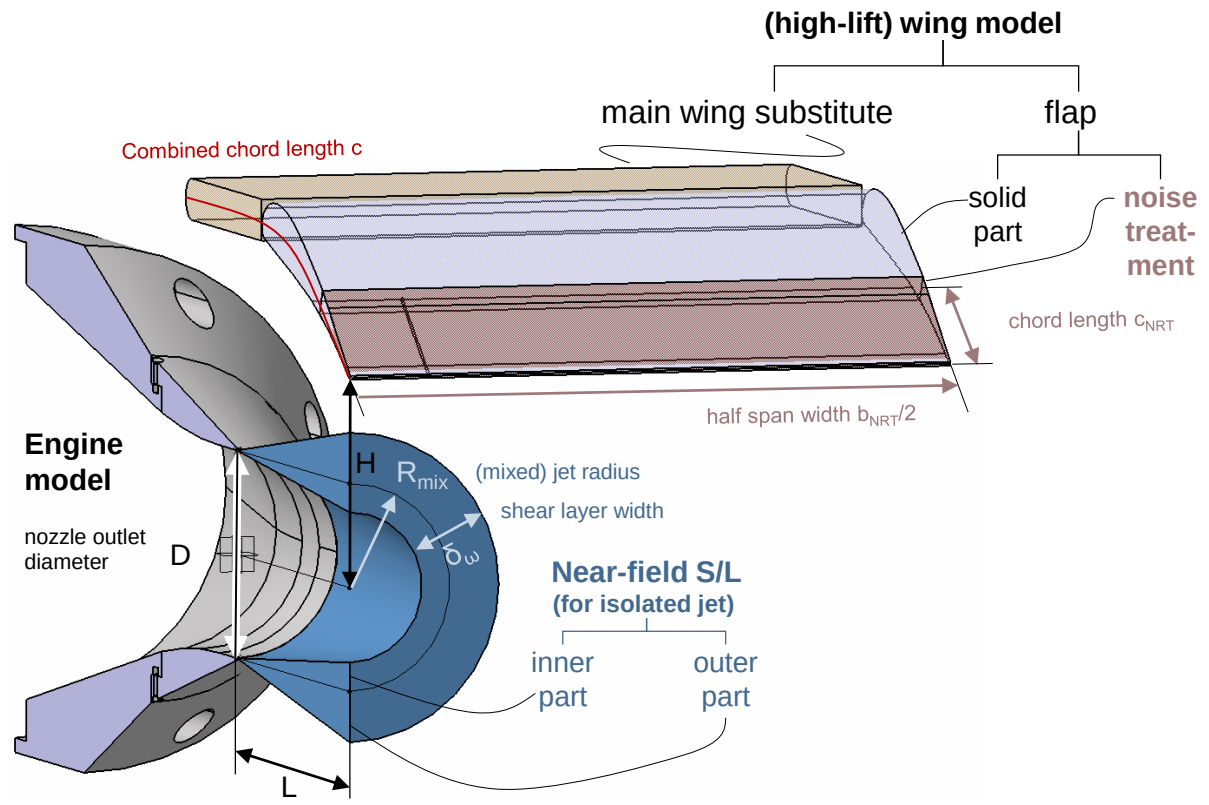

Engine integration
Length L, Height H, (Pitch, Yaw)

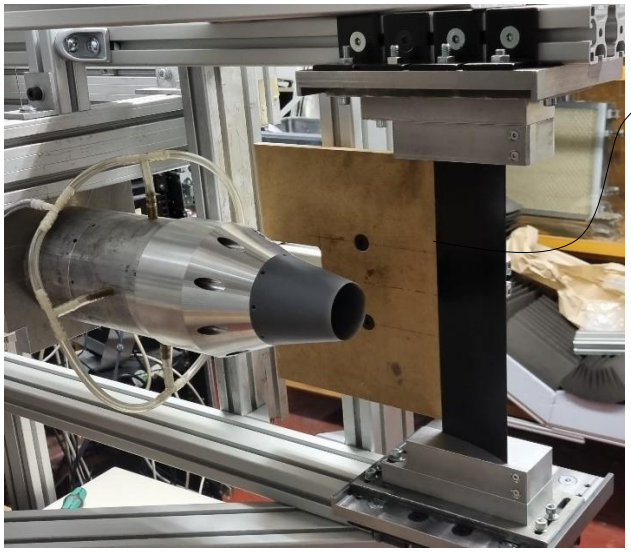

JExTRA test w/ sideways wing installation

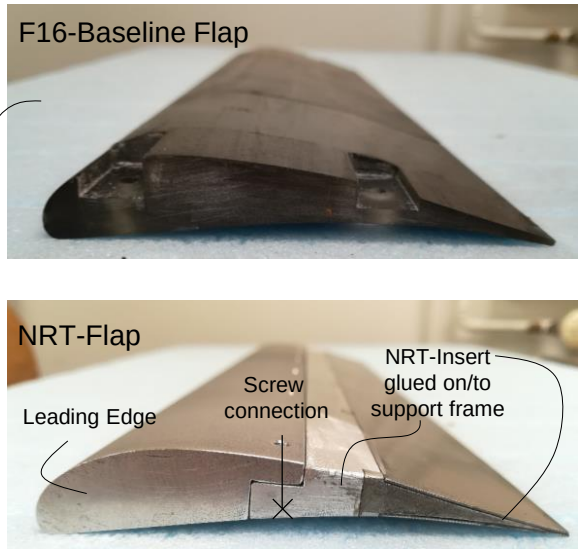

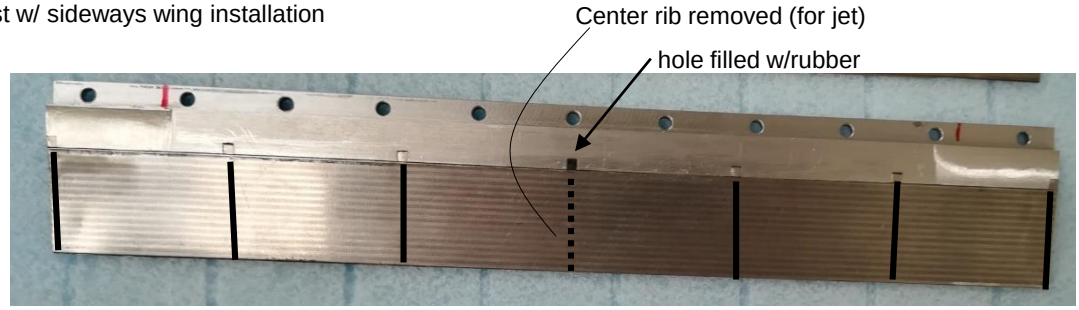

Figure 6: Implementation of NRTs for a statically operated installed engine test (single stream engine at high-lift wing) for the JExTRA experiment.

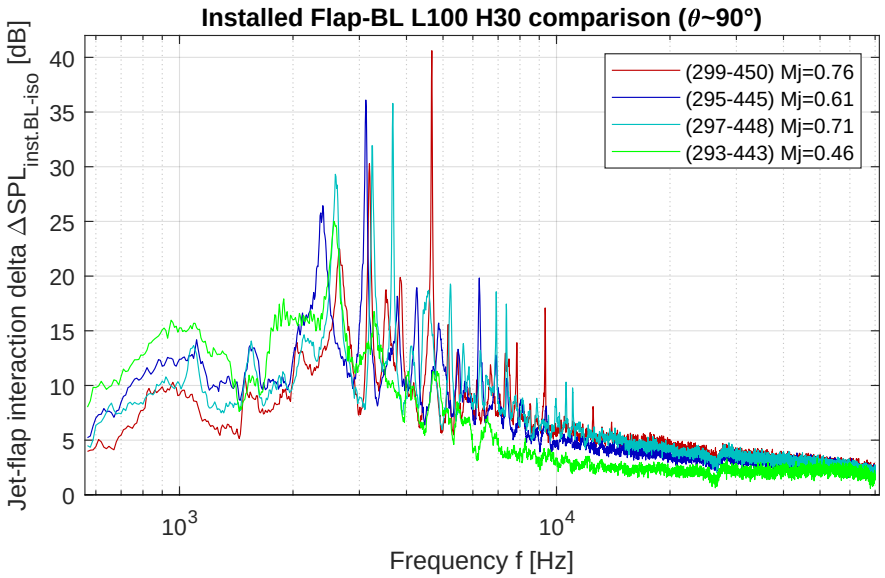

Figure 7: Static jet speed effect on JFI noise, for close engine integration ($L/D_j = 2$, $H/D_j = 0.6$), and overhead mic on flyover arc #1 ($\theta = 89\,°$, $\psi = 0\,°$)

static operation. The division is made by the presence of tonal JFI noise as well as the sensitivity wrt. changing jet speed:

- There is **low-frequent** JFI noise which interestingly decreases as jet velocity increases. It can be argued whether there are real tonal components present in this data, but it cannot be denied that there is some sort of broadband-like offset.
- The **mid-frequent** JFI noise is characterized by the presence of tones and a broadband-like peak around $He_L = 1$. The broadband-like part of the noise is approximately constant for the tested velocities.
- There is **high-frequent** JFI noise which is characterized by the absence of tones. With increasing velocity, the JFI delta increases (as expected).

The question is which frequency analogy should be used for quantifying the dividing limits between the three bands of low, mid and high frequency. Cavalieri et al. (figure 4)[6] showed that JFI noise does scale wrt. the Helmholtz analogy rather than Strouhal analogy. The Helmholtz number is defined by frequency f, characteristic length scale x as well as speed of sound of the ambient medium a_∞.

$$He_x = \frac{f \cdot x}{a_\infty} \tag{4}$$

Of particular interest is the question which length scale is universal, independent of model scale and hence problem defining. Suitable candiates are the (mixed) jet diameter D_j, the engine integration length L, the virtual engine integration length L_0 as well as the isolated jet shear layer thickness δ_ω at the position of the flap trailing edge:

$$He_{Dj} = \frac{f \cdot D_j}{a_\infty} \tag{5}$$

$$He_L = \frac{f \cdot L}{a_\infty} \tag{6}$$

$$He_{L_0} = \frac{f \cdot (L - x_{0,NF})}{a_\infty} \tag{7}$$

$$He_{\delta_\omega} = \frac{f \cdot \delta_\omega}{a_\infty} = \frac{f \cdot (L - x_{0,NF})}{a_\infty} \frac{1 - r_U}{1 + r_U} \frac{\tan(7.5\,°)}{0.64} \approx 0.21 He_{L_0} \tag{8}$$

The isolated jet shear layer thickness δ_ω at the position of the flap trailing edge is a multiple of the virtual engine integration length L_0 (see equation 8). Both properties are related by shear layer equations (amoung others derived in Jente and Delfs[7]).

Since JFI tones are generated by a feedback mechanism between nozzle lip and flap trailing edge, it can be assumed that the horizontal engine integration length L is a good fit and a promising practical value. Since the data presented in this paper was generated at a constant engine integration length, $L = 2D$, it is also possible to just use frequencies on this data set (see table 2).

	LOW-frequent	**MID-frequent**	**HIGH-frequent**
1/3 oct. band mid freq	630 ... 1600 Hz	2 ... 10 kHz	12.5 ... 63 kHz
narrowband freq. (D_j)	561 ... 1782 Hz	1782 ... 11314 Hz	1782 ... 71838 Hz
Helmholtz number He_L	0.16 ... 0.51	0.51 ... 3.2	3.2 ... 20.5
Helmholtz number He_{L^*}	0.18 ... 0.56	0.56 ... 3.6	3.6 ... 22.6

Table 2: frequency limits for low, mid and high-frequent JFI noise

For an in-depth study of JFI noise, tonal and non-tonal (or broadband-like) parts of the JFI noise are separated by using a tone removal tool. Broadband-like noise (see figure 8, top) is extracted from the spectrum by determining the median SPL value of each nth octave band. The frequency axis is separated into logarithmically equally sized bands. The bandwidth in this example is of size third-octave, i.e. each band mid frequency is spaced by factor $2^{1/6}$ to its upper and lower frequency. Within the band, the median of the sound pressure levels has been chosen as representative for the band. Choosing the median helps to decrease the influence of the magnitude of tonal components on the broadband-like value. Peaks or tonal components which have a larger bandwidth than one third-octave will be part of the broadband-like signal rather than be fully recognized as a tone (figure 8, first plot, $f = 1$ and 2.5 kHz). Therefore, in the processed data below, the bandwidth has been increased to octave used with a 50% overlap.

Once the broadband-like signal is filtered out, JFI-noise can be filtered into three components (figure 8, middle): (A) the clean broadband noise component, (B) clean tonal noise and (C) the deviation of the SPL around its mean, here described as *spectral noise*.

The question is which "clean" noise type (filtered broadband or tonal) should get the spectral noise (figure 8, bottom). The spectral noise could either remain within the tonal component (I). Then, the broadband-like noise looks very neat and it is possible to spot effects in diagrams even if four different curves are plotted. Or (II), the spectral noise is accounted as part of the broadband noise component. This is somewhat helpful since it seems that the nature of the filter loses its importance; only tones are removed from the spectrum.

The broadband-like JFI noise (II) can be evaluated by calculating the OASPL values. The JFI effect and noise reduction can be expressed in $\Delta OASPL$.

B. Analysis of noise reduction technologies wrt broadband part of JFI noise

The following sensitivity plots show in black the JFI effect (installed baseline - isolated engine) on the left y-axis. This value is also the maximum noise reduction potential (see equation 1). The achieved noise reduction is displayed in colors on the right y-axis. It is defined as installed baseline minus installed NRT equation 3). If the JFI effect is completely nullified, both curves match.

The $\Delta OASPL$ has been calculated with tones (thick) and with tones removed (thin). The rather high tones may only be measured in a very clean test environment and therefore not very suiting for practical application.

Let us first examine the sensitivity of the JFI effect figure 10, black curves) with respect to jet Mach number at an overhead microphone. The JFI effect with tones (thick) amounts to $\Delta OASPL = 12 \ldots 15$ dB and correlates with a positive sensitivity to increasing velocity. Yet, it reaches a plateau for $M_j > 0.6$.

With removed tones (thin black line) the JFI effect is smaller $\Delta OASPL \approx 10$ dB and there is even a slight negative sensitivity wrt. jet velocity. This sensitivity vastly correlates to the before defined low-frequent JFI effect (compare figure 7): In terms of broadband-like JFI deltas, the sensitivity wrt. jet Mach number is negative for low-frequent JFI noise (decreasing(!) JFI noise at increasing jet speed), rather indifferent for mid-frequent JFI noise and positive for high-frequent JFI noise. Since the low

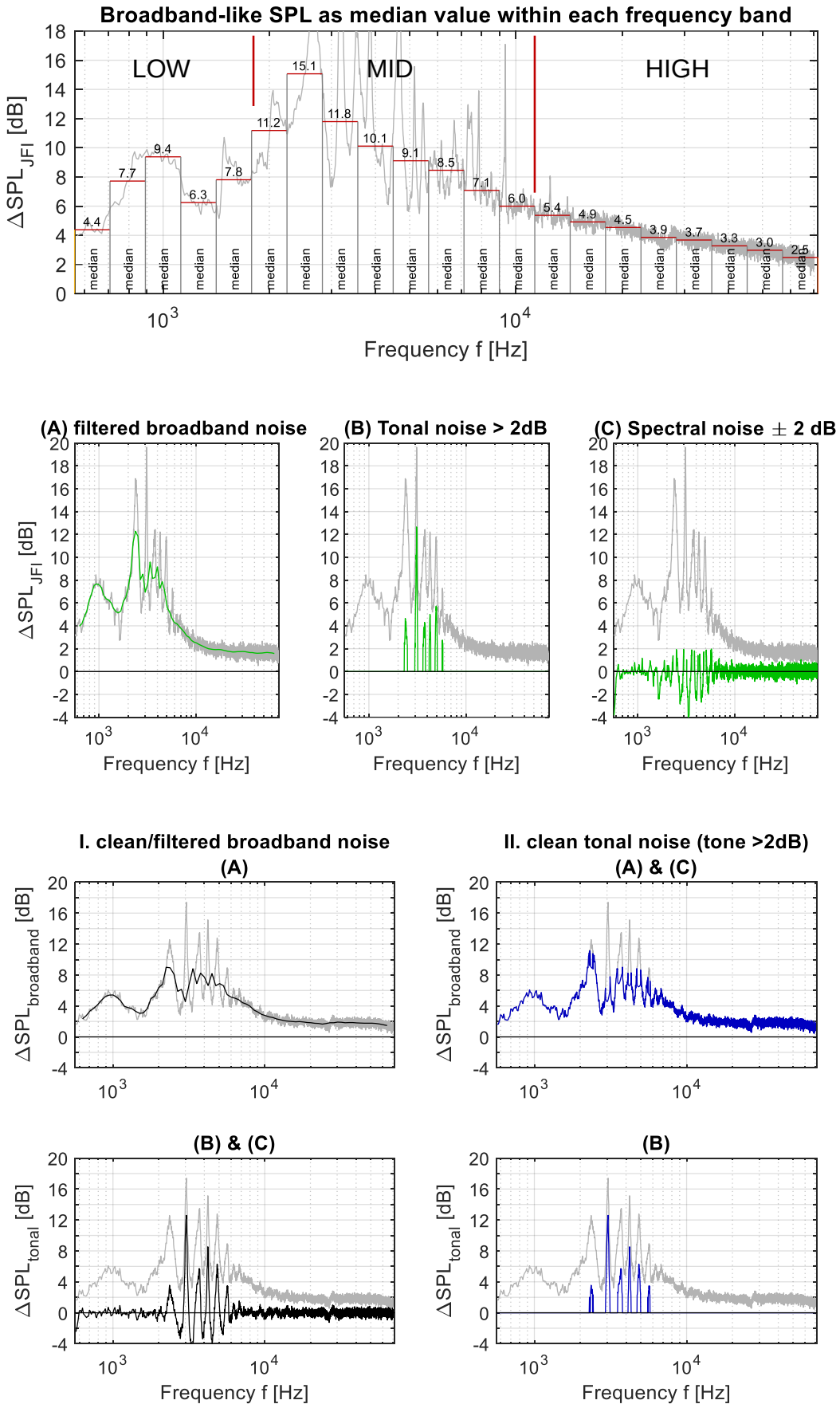

Figure 8: Evaluation method of JFI noise ΔSPL_{JFI}. top: decomposition into tonal, broadband-like and spectral noise, mid: assignment of spectral noise, bottom: determination of mean low-, mid- and high-frequent JFI noise.

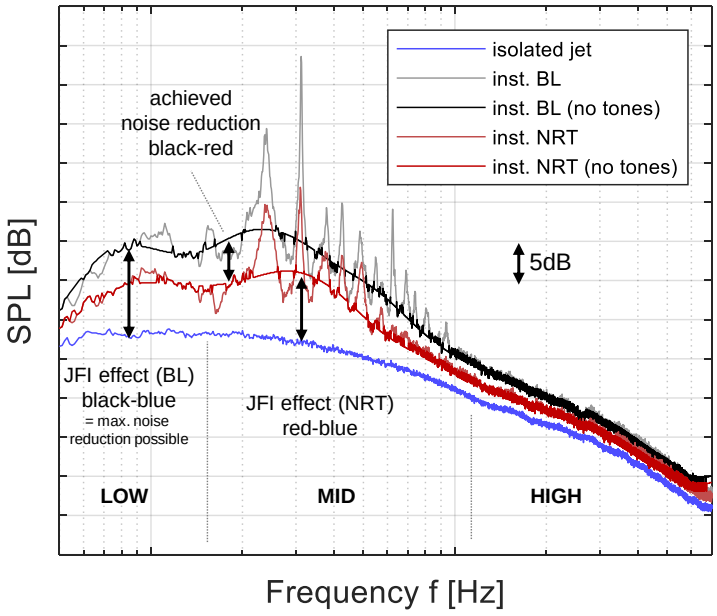

Figure 9: Installed and isolated jet noise, with and without tone removal tool

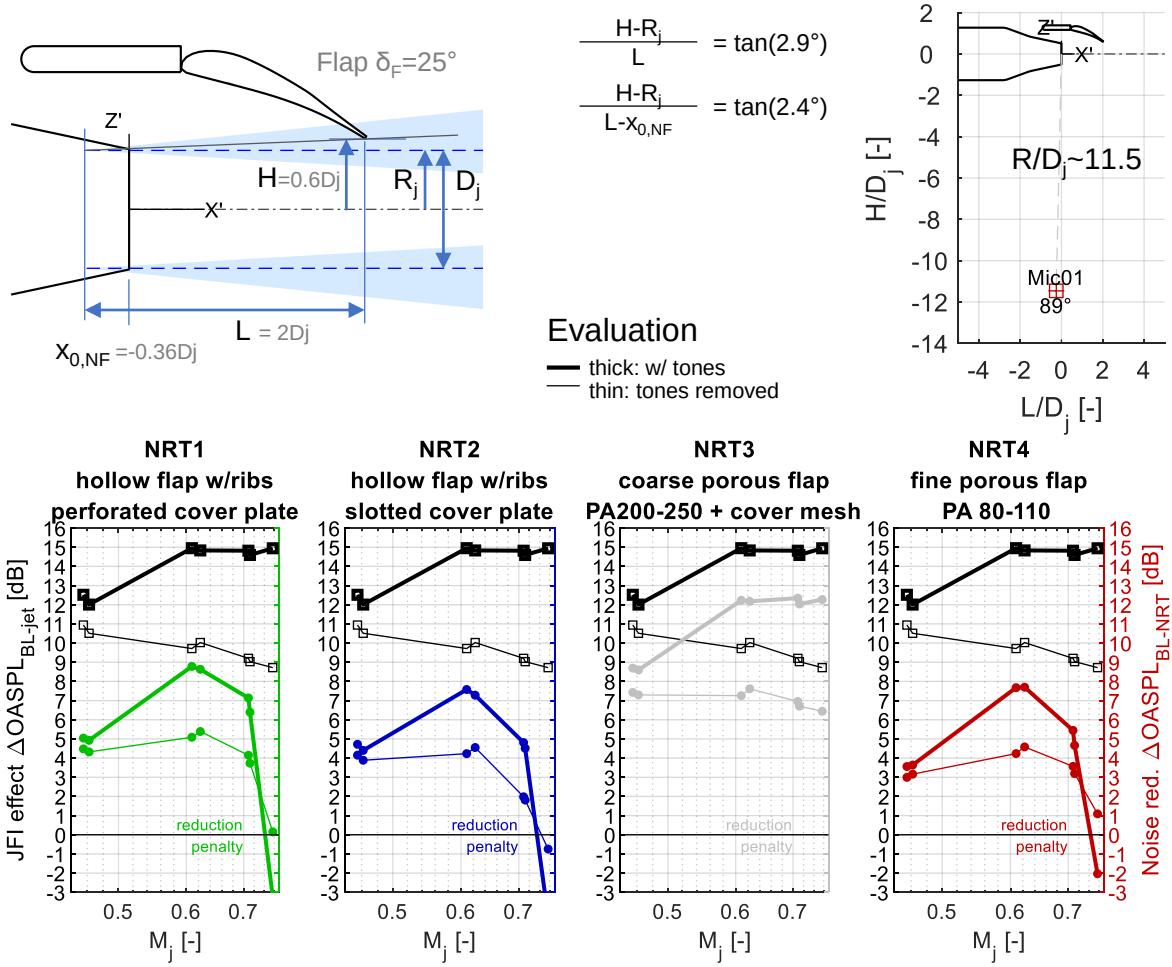

Figure 10: Static jet speed effect on JFI noise, for close engine integration ($L/D_j = 2$, $H/D_j = 0.6$), and overhead mic on flyover arc #1 ($\theta = 89\,°$, $\psi = 0\,°$)

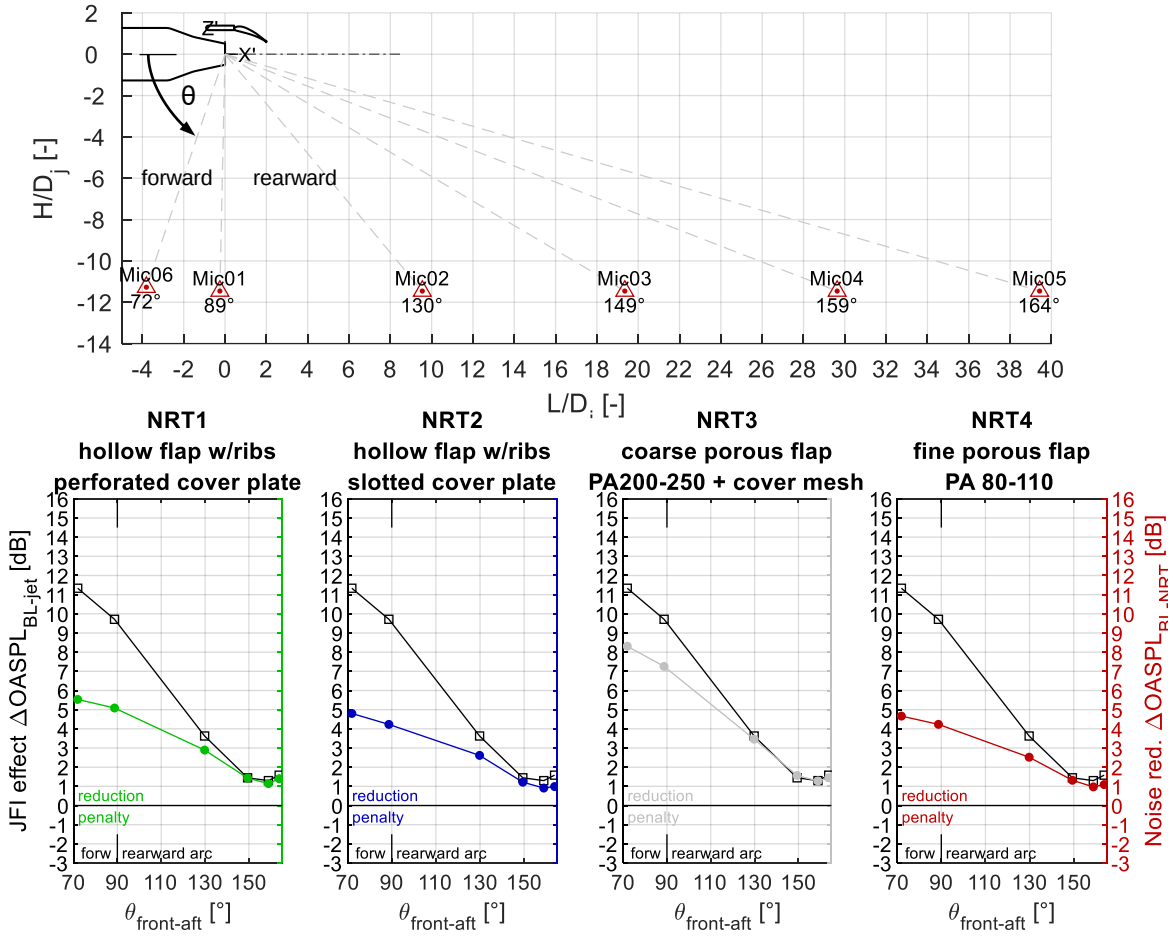

Figure 11: Polar directivity of JFI broadband noise (tones removed) along flyover arc $\psi = 0\,°$, for close engine integration ($L/D_j = 2$, $H/D_j = 0.6$), static jet operated at $M_j = 0.61$

frequency range is very high in absolute sound pressure level, changes within this region affect the OASPL calculation the most.

There is an optimal jet velocity (figure 10: $M_j \approx 0.6$) where three of the four tested noise reduction devices perform best. All NRTs (except NRT3) show a performance drop for jet speed faster than $M_j = 0.62$. Even though the JFI noise (and hence the noise reduction potential) does generally increase for higher jet speed, there is no noise reduction and even noise penalty for some NRTs at $M_j = 0.75$.

The directivity of the JFI-noise is strongest in the forward arc of the flyover position (figure 11). In absolute terms, noise reduction is also strongest in the forward arc.
Contrary to this, the JFI effect is very small in the far rearward arc, i.e. for $\theta > 150\,°$.Yet, in relative terms, the JFI effect there is almost completely nullified by the NRTs.

The azimuthal plane along the overhead position shows a symmetric directivity wrt. to the engine integration plane (figure 12). The maximum is located in the flyover plane.

C. Analysis of noise reduction technologies wrt the tonal JFI noise

Tonal JFI noise is displayed in the same color scheme as the results for broadband-like noise. The colored curves (in figure 14) show either noise reduction or penalty due to installation of an NRT. If the tones on the reduction and penalty side do approximately mirror themselves, then there is simply a tiny frequency shift in tonal JFI noise and no real reduction occurs.

The JFI noise consists of different non-harmonic tones whose origin has been explained before, among others by Jordan et al.[8] In general, the NRTs reduce more tonal JFI noise than producing new tones. However, NRT1, NRT2 and NRT4 introduce some additional tones at high jet speed. These tones follow a Helmholtz analogy: The first harmonic ($He = 1$) is visible for a jet speed of $M_j > 0.6$. For higher jet speed up to $M_j = 0.71$ additional tones show up within ($1 < He < 4$). This is a rather limited

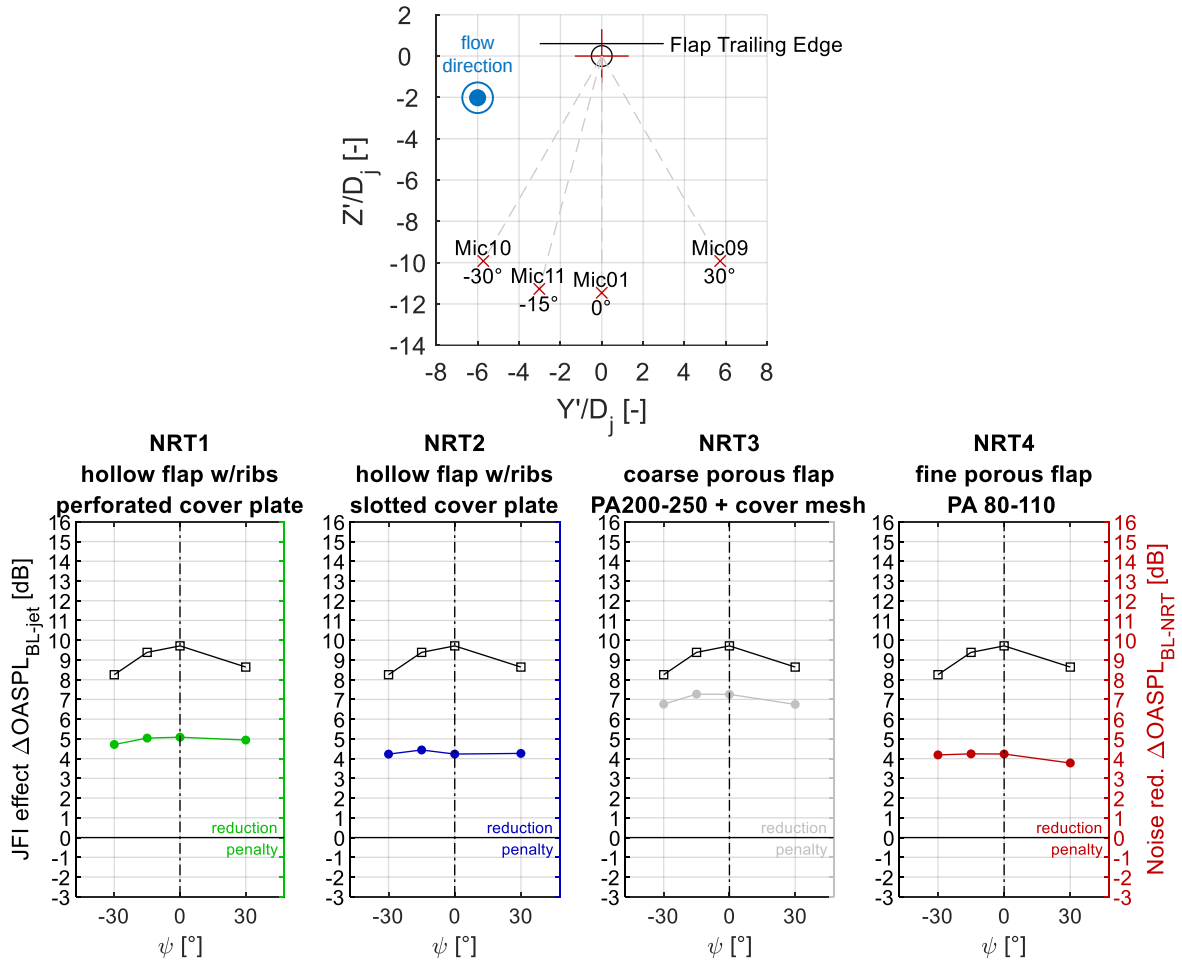

Figure 12: Azimuthal directivity of JFI broadband noise (tones removed) along overhead position $\theta = 89\,°$, for close engine integration ($L/D_j = 2$, $H/D_j = 0.6$), static jet operated at $M_j = 0.61$

range compared to the jet speed of $M_j = 0.75$, where high harmonics frequencies are visible (NRT1: 1-6, NRT2: 1-9, NRT3: none, NRT4: 1-5).

One question is why more harmonic tones can be seen for higher jet speed. Various researchers[9,10,8] have found that the jet potential core as well as the near field shear layer support different types of upstream and downstream traveling modes. With higher jet speed, there are more types of modes which can support the feedback mechanism between engine nozzle lip and flap trailing edge. This may be the reason why more harmonic tones appear for higher jet speed.

In between NRT1, NRT2 and NRT4, NRT4's irregular trailing edge does a better job than the regularly cogged, but thick trailing edges of NRT1 or NRT2. Yet, NRT3 does not show any tones for the close engine integration. The additional cover mesh is presumably the responsible mechanism which prevents the introduction of additional tones.

The data in figures 14 about the tonal JFI noise study of the noise reduction devices finds that the characteristic length for matching tones $L^* \approx 2.16 \ldots 2.26 D_j$ to whole numbers of $He = 1, 2, 3, \ldots$ is slightly larger than the engine integration length $L = 2D_j$ and smaller than the virtual engine integration length $L_0 = 2.36 D_j$ (figure 13).

The virtual integration length L_0 is the distance between the virtual shear layer origin $x_{0,NF}$ and the flap trailing edge. The virtual shear layer origin of the jet near field can be determined by a steady aerodynamics measurement. The property can be the solution to an otherwise very difficult problem, as it summarizes the imperfection of small, but finite external and internal boundary layers as well as the finite nozzle lip thickness.

For single stream engines the initial expection is that $x_{0,NF} \approx 0$. Hence, the rather large value of $x_{0,NF}/D_j = 0.36 \pm 0.04$ comes as a surprise. However, there is a very good geometric reason for this value: The inner contour of the nozzle is stricly converging in streamwise direction until $\Delta x/D_j \approx -0.32 \ldots 0$ where the nozzle is cylindric (i.e. diameter=jet diameter, see figure 6). In this last cylindrical nozzle

piece, the internal nozzle boundary layer does naturally build up in size. It makes sense that the virtual origin will minimally change along this cylindrical piece depending on jet speed.

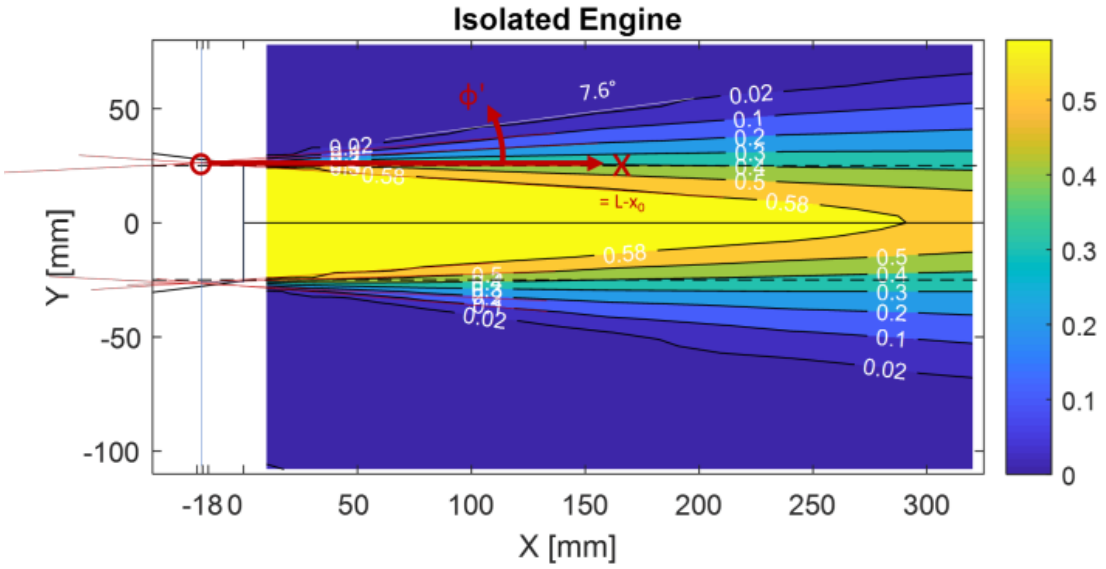

Figure 13: Construction of virtual shear layer origin of isolated jet near field at $x_{0,NF} = -18mm$ $(= -0.36D_j)$, steady aerodynamics measurement.

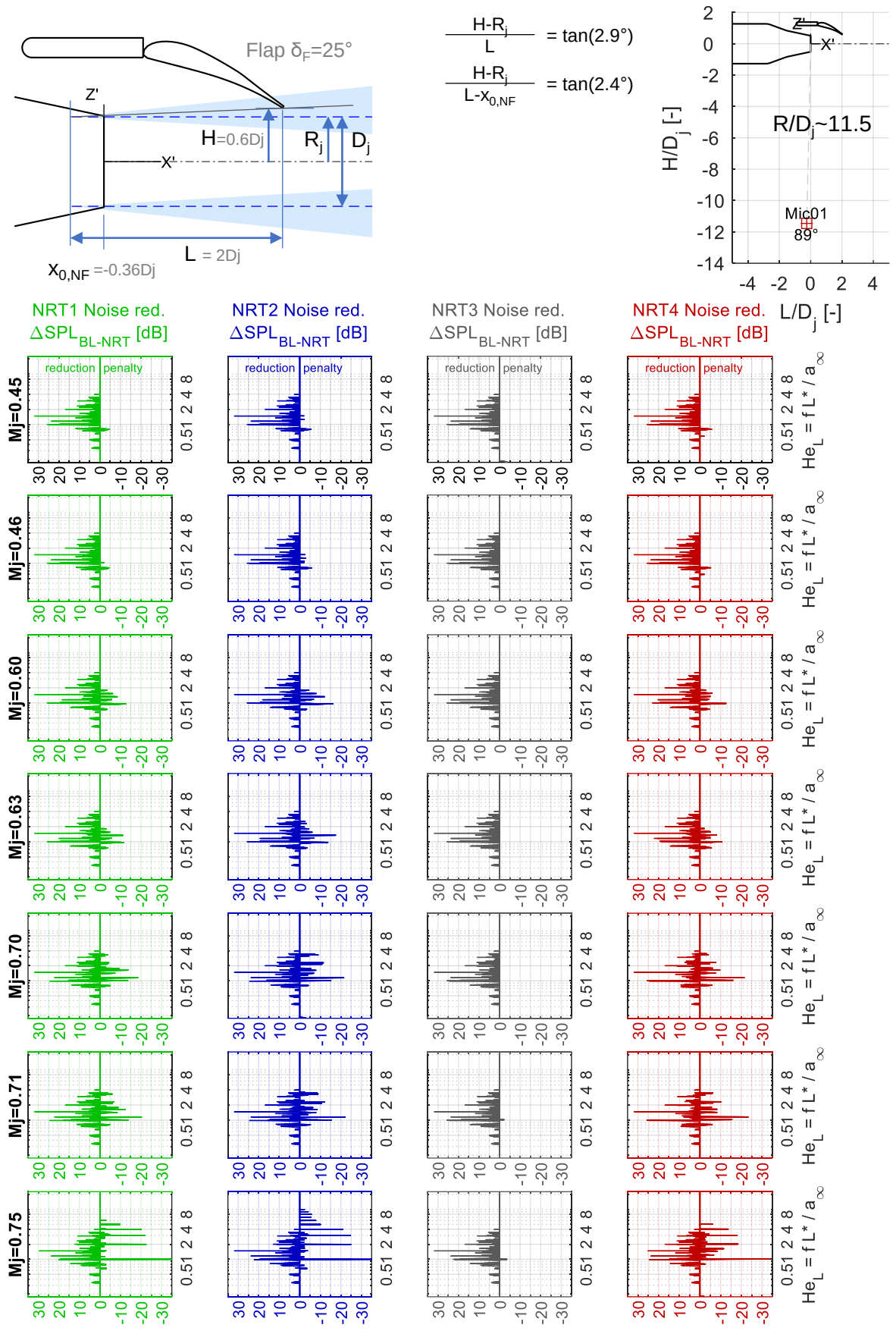

Figure 14: Static jet speed effect on tonal JFI noise, for close engine integration ($L/D_j = 2$, $H/D_j = 0.6$), and overhead mic on flyover arc #1 ($\theta = 89\,°$, $\psi = 0\,°$). The characteristical length is here $L^*/D_j = 2.16$

.

D. Discussion and Outlook

Porous materials as well as hollow flaps with rib structures and face sheets help decrease broadband and tonal components of JFI noise. Rego et al.(fig. 15)[11] integrated the pressure fluctuations on the surface, and found them to be the dominant noise source at low frequencies. A change of surface properties could explain changes in JFI noise.

Especially for high jet speed, there is a chance that new tonal noise sources are introduced which may very likely stem from the trailing edge. However, NRT3 prevents the formation of tones for the close engine integration. The reason behind this is likely not the porosity or the irregularity of the trailing edge in spanwise direction - this can been seen at NRT4 (tones up to $He = 5$ at $M_j = 0.75$).

Instead, the influence of the cover mesh should play a significant role. There are three effects which come with the installation of the mesh: (1) the change in surface property (mesh as a face sheet) on the porous part, (2) the enclosement of a very permeable cavity between porous trailing edge and mesh trailing edge, and (3) the formation of micro-serrations at the very thin mesh trailing edge.

Since NRT1 and NRT2 produce JFI tones at high jet Mach number, effect (1) can be ruled out as tone remover. Future work to deepen the understanding could focus on separating the other effects (2) and (3), if this is possible. The experimenting with cover meshes (possibly even on solid surfaces) is advised as well as a repetion of the installed engine test at the more correct mechanical engine integration height. Moreover, there is no data for the NRT performance of an installed engine setup under flight conditions.

Acknowledgments

The author wants to acknowledge the fundamental research work of DLR Braunschweig and the Institute of Fluid Mechanics (ISM) of Technische Universität Braunschweig in their collaborative research center SFB880 - *Fundamentals of High-Lift for Future Civil Aircraft*, the provision of test data on the cruise wing and their noise reduction technologies. The JExTRA test team and DLR Berlin is acknowledged for their help and support to gather installed engine data within the EU-project DJINN.

The EU DJINN (Decrease Jet Installation Noise) project receives funding from the European Union's Horizon 2020 research and innovation programme under grant agreement No 861438. DJINN is a collaborative effort between CFD-Berlin (coordinator), Airbus SAS, Dassault Aviation, Safran Aircraft Engines, Rolls-Royce Deutschland, ONERA, DLR, University of Southampton, CERFACS, Imperial College London, von Karman Institute, CNRS, and Queen Mary University of London.

References

[1]Schmidt, J., *Aeroakustische Untersuchungen an porösen Hinterkanten*, Master's thesis, Technische Universität Braunschweig, 2019.

[2]Pott-Pollenske, M. and Delfs, J., *Enhanced Capabilities of the Aeroacoustic Wind Tunnel Braunschweig*.

[3]Herr, M., Rossignol, K.-S., Delfs, J., Lippitz, N., and Mößner, M., *Specification of Porous Materials for Low-Noise Trailing-Edge Applications*.

[4]Siller, H., Nussbaumer, M., Hayat, W., Bassetti, A., Funke, S., Hage, W., and Meyer, R., "Ein kleiner Freistrahl-prüfstand für aeroakustische Messungen," *DAGA 2022 - 42. Jahrestagung für Akustik*, edited by B. Deutsche Gesellschaft für Akustik e.V. (DEGA), March 2016, pp. 363–366.

[5]Jente, C., "Strahl-Klappen-Interferenz – wie bedeutsam ist die Interaktionsschallquelle am Flugzeug," *DAGA 2022 - 48. Jahrestagung für Akustik*, edited by B. Deutsche Gesellschaft für Akustik e.V. (DEGA), April 2022, pp. 1278–1281.

[6]Cavalieri, A. V., Jordan, P., Wolf, W. R., and Gervais, Y., "Scattering of wavepackets by a flat plate in the vicinity of a turbulent jet," *Journal of Sound and Vibration*, Vol. 333, No. 24, 2014, pp. 6516–6531.

[7]Jente, C. and Delfs, J., "Velocity Scaling of Shear Layer Noise induced by cold Jet flow with co-flowing Flight stream," *25th AIAA/CEAS Aeroacoustics Conference*, Aeroacoustics Conferences, American Institute of Aeronautics and Astronautics, 2019.

[8]Jordan, P., Jaunet, V., Towne, A., Cavalieri, A. V. G., Colonius, T., Schmidt, O., and Agarwal, A., "Jet–flap interaction tones," *Journal of Fluid Mechanics*, Vol. 853, 2018, pp. 333–358.

[9]Towne, A., Cavalieri, A. V. G., Jordan, P., Colonius, T., Schmidt, O., Jaunet, V., and Brès, G. A., "Acoustic resonance in the potential core of subsonic jets," *Journal of Fluid Mechanics*, Vol. 825, 2017, pp. 1113–1152.

[10]Schmidt, O. T., Towne, A., Colonius, T., Cavalieri, A. V. G., Jordan, P., and Brès, G. A., "Wavepackets and trapped acoustic modes in a turbulent jet: Coherent structure eduction and global stability," *Journal of Fluid Mechanics*, Vol. 825, 2017, pp. 1153–1181.

[11]Rego, L., Casalino, D., Avallone, F., and Ragni, D., "Noise Amplification Effects due to Jet-Surface Interaction," *AIAA Scitech 2019 Forum*, AIAA SciTech Forum, American Institute of Aeronautics and Astronautics, 2019.